Supporting Information

Ferromagnetic Coupling in Copper Benzimidazole Chloride: Structural, Mass Spectrometry, Magnetism, and DFT Studies

Xing-Xing Shi, [+,a] *Yuexing Zhang,* [+,b] *Qiu-Jie Chen,* [+,b] *Zheng Yin,*[c] *Xue-Li Chen,*[b] *Zhenxing Wang,*[d] *Zhong-Wen Ouyang,*[d] *Mohamedally Kurmoo,*[e] *Ming-Hua Zeng*[*,a,b]

[a] Key Laboratory for the Chemistry and Molecular Engineering of Medicinal Resources, School of Chemistry and Pharmaceutical Sciences, Guangxi Normal University, Guilin, 541004, P. R. China. [b] Hubei Collaborative Innovation Center for Advanced Organic Chemical Materials, Ministry of Education Key Laboratory for the Synthesis and Application of Organic Functional Molecules, College of Chemistry and Chemical Engineering, Hubei University, Wuhan 430062, P. R. China. [c] College of Chemistry and Chemical Engineering Shaanxi University of Science and Technology, Xi'an, 710021, P. R. China. [d] Wuhan National High Magnetic Field Center & School of Physics, Huazhong University of Science and Technology, Wuhan, 430074, P. R. China. [e] Institut de Chimie de Strasbourg, CNRS-UMR 7177, Université de Strasbourg, 67070 Strasbourg, France.
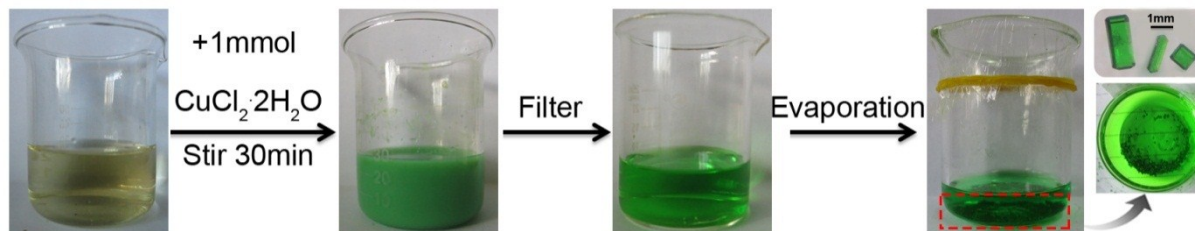
Figure S1. The synthesis procedure and photograph of **CBC** crystals.
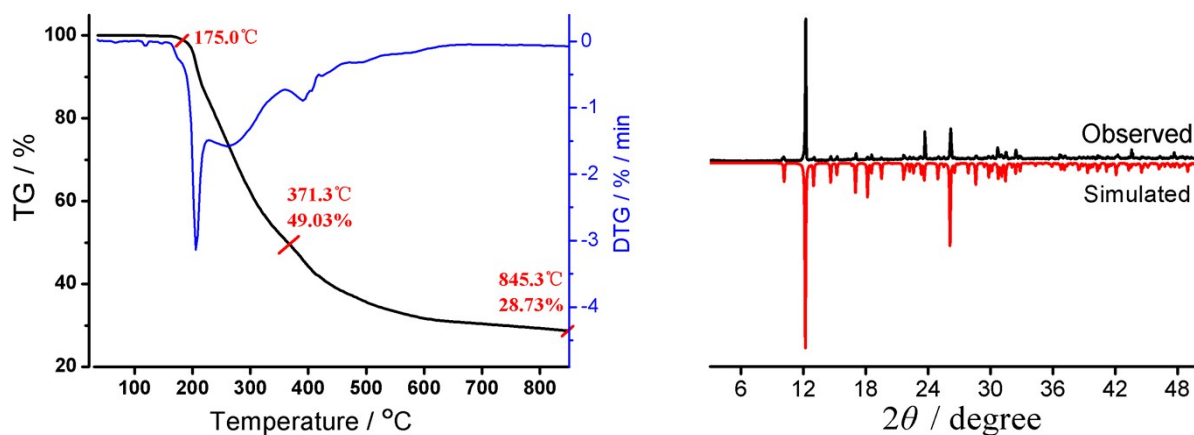

Figure S2. (Left) TGA of **CBC**. There is no weight loss until a turning point at nearly 175 °C, suggesting no solvent in the structure of **CBC**. The first weight loss of 50.9% from 175 °C to 370 °C corresponds to the departure decomposition of the H*mbm* ligand (Calc. 54.6%). The residue may be CuO with residuals of 28.7% (Calc. 26.8 %). (Right) Experimental and simulated PXRD patterns for **CBC**.

Table S1. Crystal and structure refinement data for **CBC** at 296 and 90 K.

	CBC (296 K)	**CBC** (90 K)
Formula	$C_9H_{10}Cl_2CuN_2O$	$C_9H_{10}Cl_2CuN_2O$
Weight	296.63	296.63
Crystal System	monoclinic	monoclinic
Space Group	$P\,2_1/n$	$P\,2_1/n$
a (Å)	9.752(3)	9.723(3)
b (Å)	7.817(2)	7.711(3)
c (Å)	14.238(4)	14.121(5)
β (°)	101.21(3)	101.44(4)
V (Å^3)	1064.7(5)	1037.72(6)
Z	4	4
D_c (g·cm^{-3})	1.851	1.899
F (000)	596	596
μ (mm^{-1})	2.524	2.589
Reflection collected	15478	4778
Unique Reflection	3171	2475
R_{int}	0.0321	0.0259
$R_1{}^a$, $wR_2{}^b$ [I > 2σ(I)]	0.0249/0.0610	0.0302/0.0654
R_1, wR_2 (all data)	0.0287/0.0633	0.0340/0.0682
GOF	1.093	1.070
H-atom treatment	refall	refall
Δρ$_{max}$, Δρ$_{min}$, (e Å^{-3})	0.311, −0.452	0.533, -0.467

[a] $R_1=\Sigma||F_o|-|F_c||/\Sigma|F_o|$, [b] $wR_2=[\Sigma w(F_o{}^2-F_c{}^2)^2/\Sigma w(F_o{}^2)^2]^{1/2}$.

Table S2. Cell parameters, selected bond lengths (Å) and angles (°) for **CBC** at 296 and 90 K.

	CBC(296 K)	CBC(90 K)	Max. deviation [a]
a / Å	9.752(3)	9.723(3)	0.30%
b / Å	7.817(2)	7.711(3)	1.36%
c / Å	14.238(4)	14.121(5)	0.82%
β (°)	101.21(3)	101.44(4)	-0.23%
V / Å^3	1064.7(5)	1037.72(6)	2.53%
Cu(1)-N(1)	1.970(12)	1.969(18)	0.05%
Cu(1)-Cl(1)	2.251(6)	2.253(6)	-0.09%
Cu(1)-O(1)	2.071(12)	2.062(16)	0.43%
Cu(1)-Cl(2)	2.225(6)	2.228(6)	-0.13%
Cu···Cl	2.998(8)	2.948(6)	1.67%
Cu···Cu	4.581(9)	4.543(4)	0.83%
N(1)-Cu(1)-O(1)	80.58(5)	80.86(7)	-0.35%
O(1)-Cu(1)-Cl(1)	172.65(4)	173.14(5)	0.28%
O(1)-Cu(1)-Cl(2)	86.95(4)	86.88(5)	0.08%
C(8)-O(1)-Cu(1)	115.67(9)	115.60(13)	0.06%
C(2)-N(1)-Cu(1)	114.71(10)	114.54(15)	0.15%
N(1)-Cu(1)-Cl(1)	100.08(4)	99.81(5)	0.27%
N(1)-Cu(1)-Cl(2)	158.97(4)	159.46(6)	-0.31%
Cl(2)-Cu(1)-Cl(1)	94.45(2)	94.33(2)	0.13%
Cu(1)-O(1)-H(1)	110.7(16)	109.0(2)	1.5%
C(3)-N(1)-Cu(1)	139.24(10)	139.39(15)	-0.11%
Cu(1)-Cl(1) ···Cu	121.84(8)	122.13(6)	-0.24%
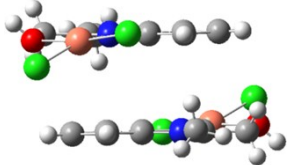
[a]Max. deviation = [**CBC**(296 K)-**CBC**(90 K)]/Max.{**CBC**(296 K), **CBC**(90 K)}
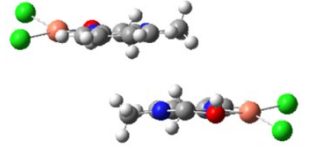
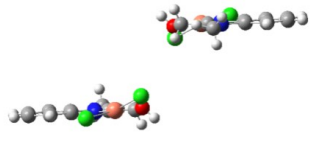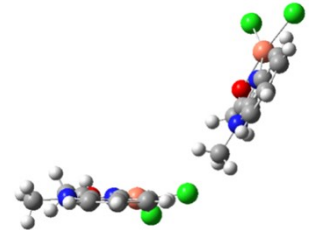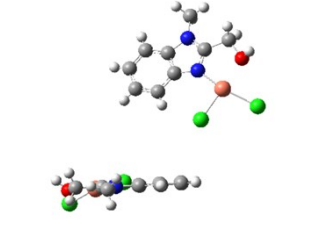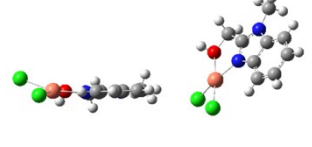**Table S3.** The CShM values calculated by SHAPE 2.0 for **CBC**.

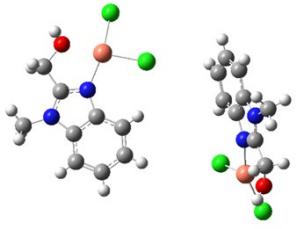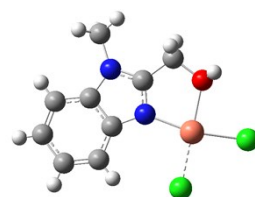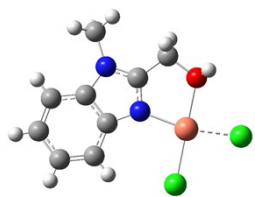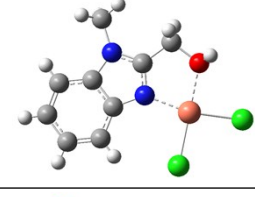|	CBC_90 K	CBC_296 K	Ideal structures
4_Coordination	**1.825**	**1.910**	Square
	24.731	24.419	Tetrahedron
	12.631	12.418	Seesaw or sawhorse[a] (*cis*-divacant octahedron)

[a] A regular polyhedron with one or two vertices removed.

Table S4 Calculated complexation energies without and after basis set superposition errors correction (BSSE) (CE and CE-BSSE, in kcal/mol) between **CBC** monomer and its all possible neighbors in **CBC** crystals, the magnetic interaction J between Cu atoms in some dimers are also given. Interaction schemes of negative complexation energy smaller than -4 kcal/mol and positive complexation energy are not given.

	Method	CE	CE-BSSE	J /cm^{-1}	Interaction Types and Scheme
dimer67_14	B3LYP-D3/(6-311G*,SDD)	-39.64	-35.16	0.04	$PhC_3N_2 \cdots PhC_3N_2$ (3.525, 3.339)
	B3LYP-D3/TZVP	-38.6	-34.68	0.04	
	B97D-D3/(6-311G*,SDD)	-38.47	-34.1	0.19	
	B97D-D3/TZVP	-37.45	-33.61	0.16	
dimer38_14	B3LYP-D3/(6-311G*,SDD)	-19.84	-17.63	3.58	Cl1a$\cdots$H-O1 (3.094), Cl2a$\cdots$Cu1 (2.998)
	B3LYP-D3/TZVP	-19.64	-17.92	4.46	
	B97D-D3/(6-311G*,SDD)	-18.47	-16.27	-33.38	
	B97D-D3/TZVP	-18.41	-16.64	-63.60	
	LC-BLYP/(6-311G*,SDD)	-18.07	-15.72	1.18	
	LC-BLYP/TZVP	-17.48	-15.76	1.23	
	ωB97XD/(6-311G*,SDD)	-18.50	-16.30	1.45	
	□ωB97XD/TZVP	-17.73	-16.25	1.46	
dimer64_14	B3LYP-D3/(6-311G*,SDD)	-13.98	-12.26	0.001	2 $PhC_3N_2 \cdots CH_3$ (3.516)
	B3LYP-D3/TZVP	-13.2	-12.18	0.001	

	B97D-D3/(6-311G*,SDD)	-14.81	-13.13	0.005	
	B97D-D3/TZVP	-13.87	-12.91	0.003	
dimer58_14	B3LYP-D3/(6-311G*,SDD)	-13.48	-13.12	-0.01	2 Cl2a⋯CH$_2$(4.799)
	B3LYP-D3/TZVP	-13.30	-12.78	-0.01	
	B97D-D3/(6-311G*,SDD)	-12.56	-12.19	-0.05	
	B97D-D3/TZVP	-12.46	-11.97	-0.04	
dimer95_14	B3LYP-D3/(6-311G*,SDD)	-11.41	-10.94	-0.08	Cl1a⋯C(Me)−H(3.774) Cl1a⋯CH$_2$(3.843)
	B3LYP-D3/TZVP	-11.56	-11.01	-0.08	
	B97D-D3/(6-311G*,SDD)	-10.78	-10.30	-19.98	
	B97D-D3/TZVP	-11	-10.47	-25.00	
dimer47_14	B3LYP-D3/(6-311G*,SDD)	-4.65	-4.25	-0.003	
	B3LYP-D3/TZVP	-4.52	-4.09	-0.002	
	B97D-D3/(6-311G*,SDD)	-4.72	-4.33	-0.004	
	B97D-D3/TZVP	-4.6	-4.17	0	
dimer94_14	B3LYP-D3/(6-311G*,SDD)	-9.73	-9.06	-0.001	
	B3LYP-D3/TZVP	-10.17	-9.14	0.001	
	B97D-D3/(6-311G*,SDD)	-9.23	-8.55	-5.14	
	B97D-D3/TZVP	-9.67	-8.66	-8.70	
	LC-BLYP/(6-311G*,SDD)	-8.45	-7.76	0.001	
	LC-BLYP/TZVP	-8.82	-7.82	0	

	ωB97XD/(6-311G*,SDD)	-9.38	-8.70	0.001	
	☐ωB97XD/TZVP	-9.54	-8.68	0.001	
dimer50_14	B3LYP-D3/(6-311G*,SDD)	-4.65	-4.25	-0.003	
	B3LYP-D3/TZVP	-4.52	-4.09	-0.001	
	B97D-D3/(6-311G*,SDD)	-4.72	-4.33	-0.003	
	B97D-D3/TZVP	-4.6	-4.17	0.001	
Cl1a_Cu	B3LYP-D3/(6-311G*,SDD)	-134.12	-131.68		
	B3LYP-D3/TZVP	-139.36	-135.14		
	B97D-D3/(6-311G*,SDD)	-129.04	-126.47		
	B97D-D3/TZVP	-135.18	-130.82		
Cl2a_Cu	B3LYP-D3/(6-311G*,SDD)	-130.61	-128.26		
	B3LYP-D3/TZVP	-135.62	-132.17		
	B97D-D3/(6-311G*,SDD)	-126.39	-123.89		
	B97D-D3/TZVP	-132.28	-128.71		
CuCl2_L	B3LYP-D3/(6-311G*,SDD)	-60.27	-54.80		
	B3LYP-D3/TZVP	-54.24	--50.60		
	B97D-D3/(6-311G*,SDD)	-50.37	-44.95		
	B97D-D3/TZVP	-46.79	-42.88		
CuCl2_CuCl2L	B3LYP-D3/(6-311G*,SDD)	-12.36	-11.10	-2.55	
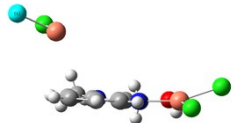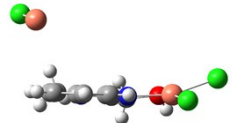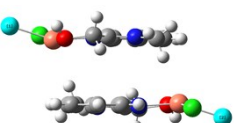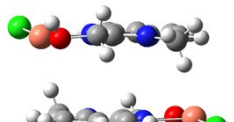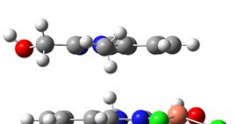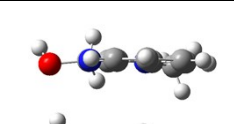
CuCl2movingCl_CuCl2L	B3LYP-D3/(6-311G*,SDD)	-12.10	-11.05	-0.22	
CuCl_CuCl2L	B3LYP-D3/(6-311G*,SDD)	-56.76	-55.71	-269.30	
CuCl2LmovingCl_CuCl2LmovingCl	B3LYP-D3/(6-311G*,SDD)	-35.47	-31.44	-0.016	
CuClL_CuClL	B3LYP-D3/(6-311G*,SDD)	21.38	24.93	-0.02	
L_CuCl2LmovingCl	B3LYP-D3/(6-311G*,SDD)	-24.55	-20.53		
L_L	B3LYP-D3/(6-311G*,SDD)	-11.80	-7.94		

Table S5. Bond order analysis of **CBC**. Atomic labels are shown below the table.

	Bond length	Mayer bond order analysis	Wiberg bond order analysis in Lowdin orthogonalized basis	Fuzzy bond order analysis	Laplacian bond order
Cu1-Cl2	2.25087	0.726732	1.40226375	1.270805	0.349608
Cu1-Cl3	2.22487	0.850844	1.44325973	1.278124	0.355882
Cu1-N6	1.96971	0.408214	0.71233414	0.973899	0.349206
Cu1-O4	2.06935	0.247506	0.55525315	0.802346	0.119568
Cu26-Cl27	2.25087	0.787143	1.45264801	1.280576	0.350855
Cu26-Cl28	2.22488	0.819988	1.50536019	1.314167	0.384987
Cu26-N31	1.96971	0.358329	0.68469556	0.945115	0.352326
Cu26-O29	2.06935	0.239623	0.53960702	0.784938	0.113537
Cl3⋯Cu26	2.99865	0.072951	0.35420619	0.321205	0.03227728
Cl2⋯H30	2.23035	0.050834	0.10228399	0.090567	0.00005362
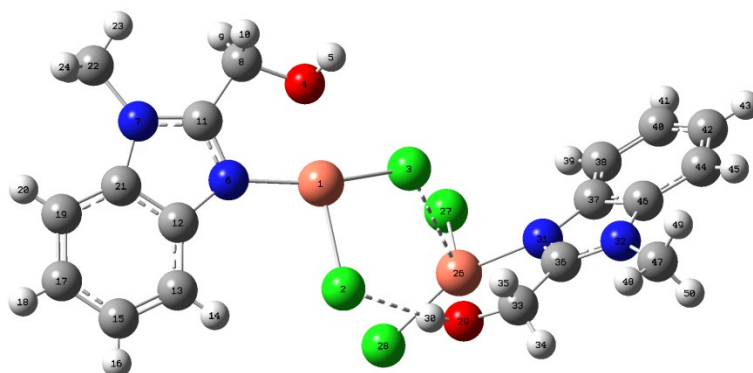
Table S6. List of H-bonds, C−H⋯π and π⋯π interactions for **CBC**.

H-bond	Distance[a], Å	Distance[b], Å	Angle[e], °	Complexation energy[f], kcal/mol
Cu1⋯Cl2a−Cu	2.998(8)	2.998(8)	121.84(19)	-17.63
O1−H⋯Cl1a*i*	3.094(14)	2.304(23)	178.67(21)	
C-H⋯Cl2a*ii*	4.799(17)	3.865(18)	165.96(17)	-13.12/2
π⋯π [g]	**Distance[c], Å**	**Distance[d], Å**		
PhC$_3$N$_2$⋯PhC$_3$N$_2$	3.525(7)	3.339(6)		-35.16
C(Me)-H⋯π	**Distance[c], Å**	**Distance[b], Å**	**Angle[e], °**	
C(Me)-H⋯π(PhC$_3$N$_2$)	3.516(24)	3.018(25)	113.09(16)	-13.12/2

Symmetric code: *i*) 1-x, -y, -z; *ii*) 1-x, -y, 1-z.
[a]Distance between acceptor and donor; [b]Distance between acceptor and H; [c]Centroid-to- centroid distance; [d] Interplanar distance; [e]Angle of acceptor-hydrogen-donor; [f]Complexation energies were calculated using B3LYP functional with BSSE correction; [g] the interaction between two CBC molecules infact including other types of interaction involving Cu⋯π and Cl⋯CH(Ph).
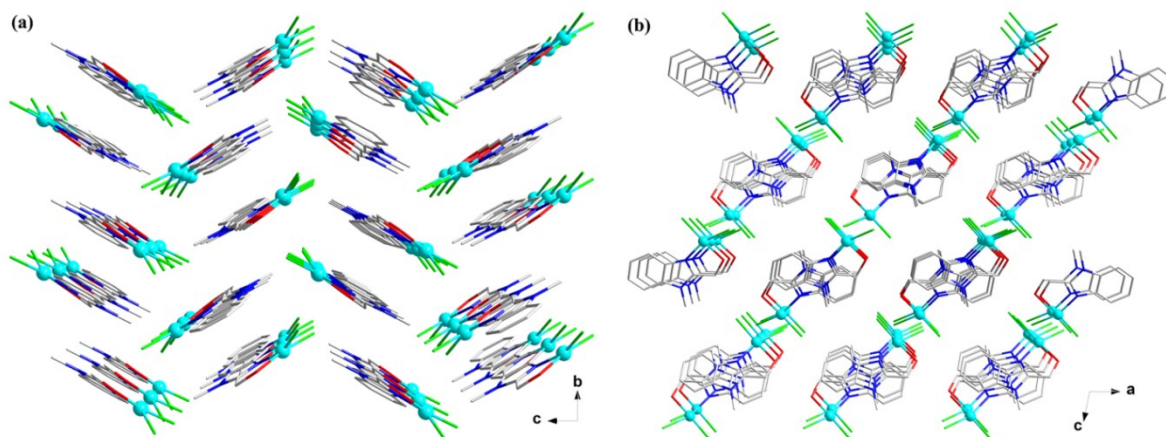
Figure S3. View of the 3D packing structure of **CBC** along the *b* axis.

a. ΔE₁ = -35.16Kcal/mol   b. ΔE₂ = -17.63Kcal/mol

c. ΔE₃ = -13.12Kcal/mol   d. ΔE₄ = -13.12Kcal/mol
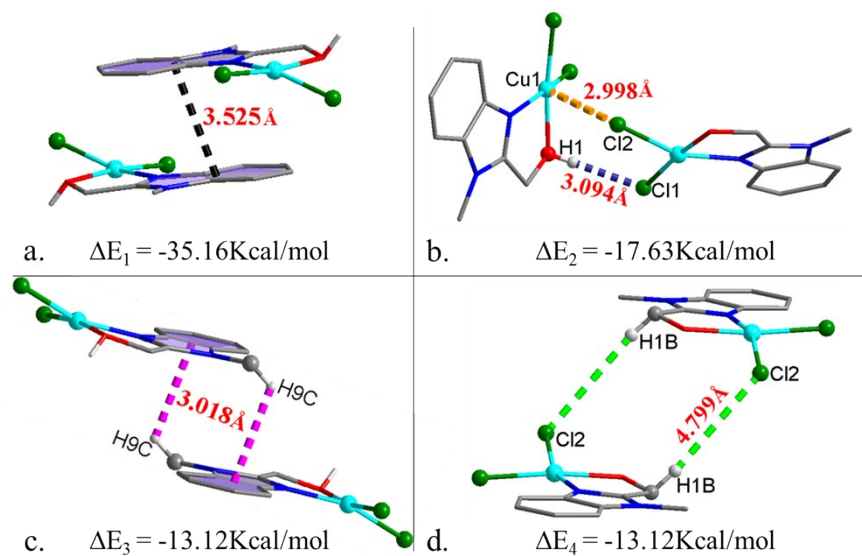
Figure S4. Intermolecular interactions in the structure of **CBC**. (a) $\pi(PhC_3N_2)\cdots\pi(PhC_3N_2)$ (dark dotted line); (b) Cu1···Cl2a (light orange dotted line); H1···Cl1a (indigo red dotted line); (c) C−H···$\pi(PhC_3N_2)$ (pink dotted line) ; (d) H1B···Cl2a (bright green dotted line) , ΔE is calculated complexation energy between different **CBC**.
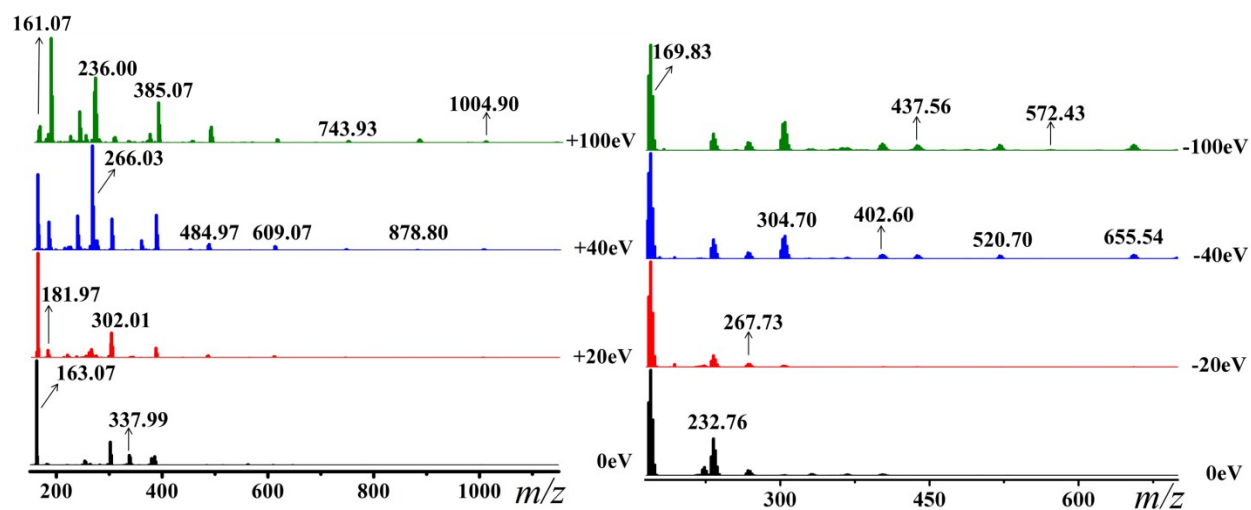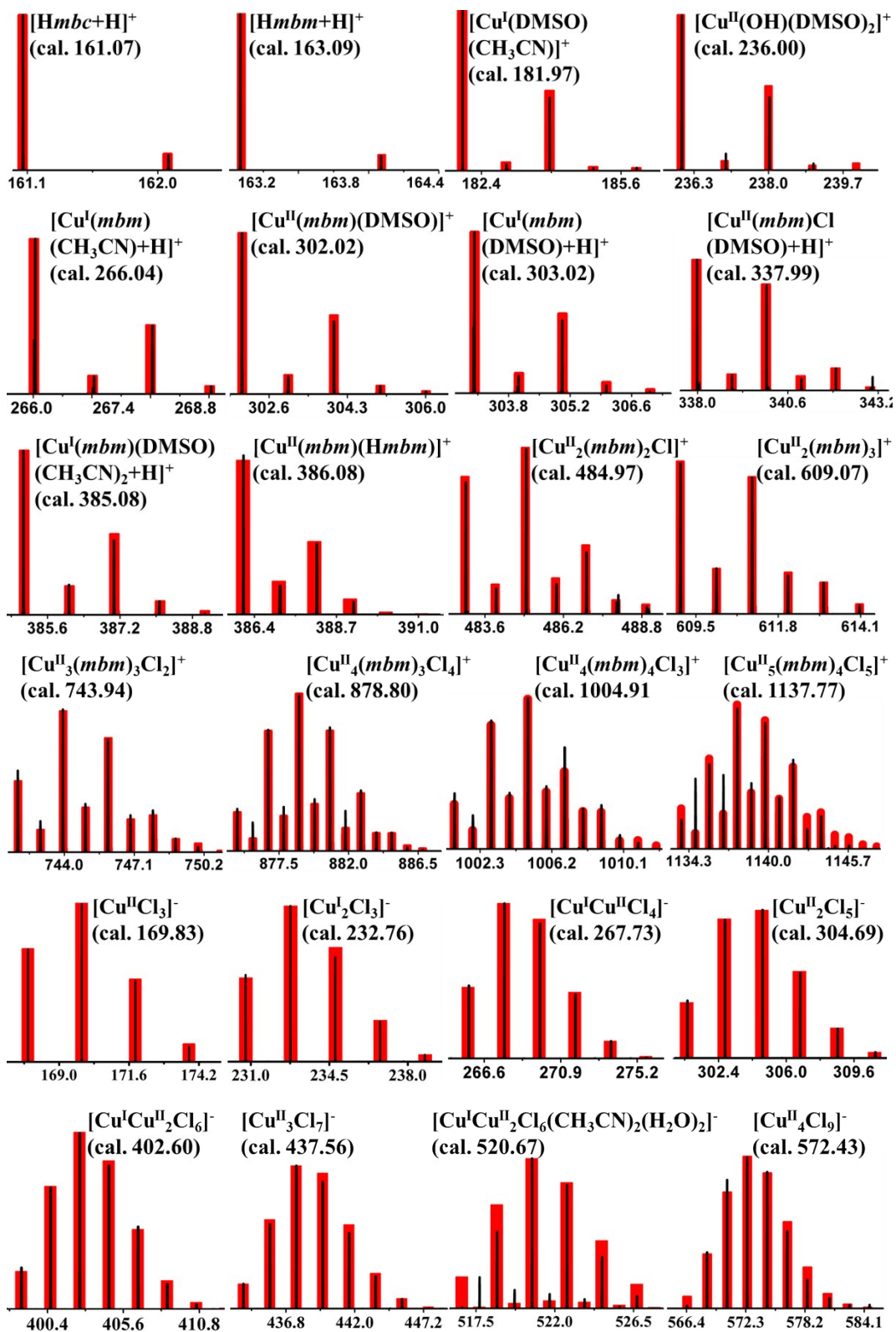

Figure S5. The positive mode (left) and negative mode (right) ESI-MS of **CBC** for different in-source energies of 0, 20, 40 and 100 eV. The crystals were dissolved in DMSO and diluted by CH_3CN for ESI-MS measurements.

Table S7. Peak assignments, relative intensity and R deviation of the ESI-MS spectrum of **CBC** under different in-source energy.

m/z of the peak	Fragment	Relative Intensity / R[a] (%)			
		0eV (R)	20eV	40eV	100eV (R)
Positive Mode					
161.07	$[(Hmbc)+H]^+$ (161.07)	1.6	6.2	72.7	16.2 (0.2)
163.07	$[Hmbm+H]^+$ (163.09)	100 (0.63)	100	15.1	0
181.97	$[Cu^I(DMSO)(CH_3CN)]^+$ (181.97)	1.6	7.7	27.6	100 (4.27)
236.02	$[Cu^{II}(OH)(DMSO)_2]^+$ (236.00)	0.3	1.7	33.5	30.3 (10.33)
266.03	$[Cu^I(mbm)(CH_3CN)+H]^+$ (266.04)	0.7	3.6	23.2	62.4 (0.89)
302.01	$[Cu^{II}(mbm)(DMSO)]^+$ (302.02)	22.7 (3.28)	24.2	0	0
303.02	$[Cu^I(mbm)(DMSO)+H]^+$ (303.02)	0	0	0	5.9 (4.73)
337.99	$[Cu^{II}(mbm)Cl(DMSO)+H]^+$ (337.99)	10.1 (1.39)	1.1	0	0
385.07	$[Cu^I(mbm)(DMSO)(CH_3CN)_2+H]^+$ (385.08)	0	0	34.0	38.7 (3.28)
386.08	$[Cu^{II}(mbm)(Hmbm)]^+$ (386.08)	8.9	9.8 (2.21)	0	0
484.97	$[Cu^{II}_2(mbm)_2Cl]^+$ (484.97)	0.4	2.6	6.5	15.7 (5.58)
609.07	$[Cu^{II}_2(mbm)_3]^+$ (609.07)	0.5	1.7	4.3	3.8 (1.40)
743.93	$[Cu^{II}_3(mbm)_3Cl_2]^+$ (743.94)	0	0.5	1.4	2.2 (7.52)
878.80	$[Cu^{II}_4(mbm)_3Cl_4]^+$ (878.80)	0	0	0.6	3.6 (10.54)
1004.90	$[Cu^{II}_4(mbm)_4Cl_3]^+$ (1004.91)	0.2	0.5	1.3	1.8 (7.27)
1137.77	$[Cu^{II}_5(mbm)_4Cl_5]^+$ (1137.77)	0.3	1.7	1	0.6 (35.10)
Negative Mode					
169.83	$[Cu^{II}Cl_3]^-$ (169.83)	100 (1.69)	100	100	100 (1.13)
232.76	$[Cu^I_2Cl_3]^-$ (232.76)	16.15	11.63	18.78	15.99 (3.62)
267.73	$[Cu^ICu^{II}Cl_4]^-$ (267.73)	5.21	3.54	6.40	8.18 (3.28)
304.70	$[Cu^{II}_2Cl_5]^-$ (304.69)	0.76	1.78	22.20	26.72 (4.53)
402.60	$[Cu^ICu^{II}_2Cl_6]^-$ (402.60)	6.78	0.39	4.26	6.71 (9.92)
437.56	$[Cu^{II}_3Cl_7]^-$ (437.56)	0	0	0.25	5.16 (14.79)
520.70	$[Cu^ICu^{II}_2Cl_6(CH_3CN)_2(H_2O)_2]^-$ (520.67)	0	0	3.43	5.70 (21.36)
572.43	$[Cu^{II}_4Cl_9]^-$ (572.43)	0	0	0	0.74 (12.36)
655.54	$[Cu^I Cu^{II}_3Cl_8(CH_3CN)_2(H_2O)_2]^-$ (655.56)	0	0	4.13	5.81 (24.52)

[a] R is a convenient index of the match between the observed and calculated MS data. *R* factor was defined as *R* = (Σ{|Iobs − Ical | / Ical})/100. Iobs and Ical are the observed and calculated intensity of each single peak at m/z, respectively.[1]

[1] S. A. R. Knox, J. W. Koepke, M. A. Andrews, H. D. Kaesz, *J. Am. Chem. Soc.* **1975**, *97*, 3942-3947.
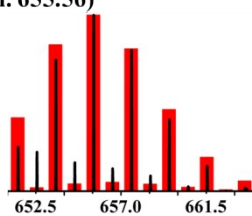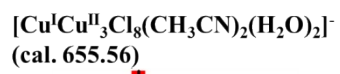
[H*mbc*+H]⁺
(cal. 161.07)

[H*mbm*+H]⁺
(cal. 163.09)

[Cuᴵ(DMSO)(CH₃CN)]⁺
(cal. 181.97)

[Cuᴵᴵ(OH)(DMSO)₂]⁺
(cal. 236.00)

[Cuᴵ(*mbm*)(CH₃CN)+H]⁺
(cal. 266.04)

[Cuᴵᴵ(*mbm*)(DMSO)]⁺
(cal. 302.02)

[Cuᴵ(*mbm*)(DMSO)+H]⁺
(cal. 303.02)

[Cuᴵᴵ(*mbm*)Cl(DMSO)+H]⁺
(cal. 337.99)

[Cuᴵ(*mbm*)(DMSO)(CH₃CN)₂+H]⁺
(cal. 385.08)

[Cuᴵᴵ(*mbm*)(H*mbm*)]⁺
(cal. 386.08)

[Cuᴵᴵ₂(*mbm*)₂Cl]⁺
(cal. 484.97)

[Cuᴵᴵ₂(*mbm*)₃]⁺
(cal. 609.07)

[Cuᴵᴵ₃(*mbm*)₃Cl₂]⁺
(cal. 743.94)

[Cuᴵᴵ₄(*mbm*)₃Cl₄]⁺
(cal. 878.80)

[Cuᴵᴵ₄(*mbm*)₄Cl₃]⁺
(cal. 1004.91

[Cuᴵᴵ₅(*mbm*)₄Cl₅]⁺
(cal. 1137.77)

[CuᴵᴵCl₃]⁻
(cal. 169.83)

[Cuᴵ₂Cl₃]⁻
(cal. 232.76)

[CuᴵCuᴵᴵCl₄]⁻
(cal. 267.73)

[Cuᴵᴵ₂Cl₅]⁻
(cal. 304.69)

[CuᴵCuᴵᴵ₂Cl₆]⁻
(cal. 402.60)

[Cuᴵᴵ₃Cl₇]⁻
(cal. 437.56)

[CuᴵCuᴵᴵ₂Cl₆(CH₃CN)₂(H₂O)₂]⁻
(cal. 520.67)

[Cuᴵᴵ₄Cl₉]⁻
(cal. 572.43)

$[Cu^ICu^{II}_3Cl_8(CH_3CN)_2(H_2O)_2]^-$
(cal. 655.56)

652.5   657.0   661.5

Figure S6. The experimental and calculated MS spectra of different fragments.

Table S8. Hirshfeld surfaces mapped with d_{norm} (left) showing Shape-index (middle) and Curvedness (right) for the **CBC**. Hirshfeld surface analysis were performed using CrystalExplorer (Version 3.1), S. K. Wolff, D. J. Grimwood, J. J. McKinnon, M. J. Turner, D. Jayatilaka, M. A. Spackman, University of Western Australia, 2012.
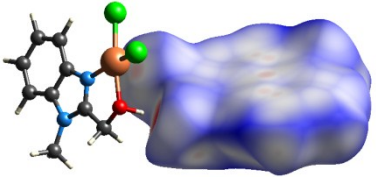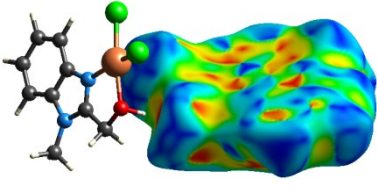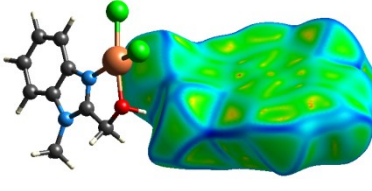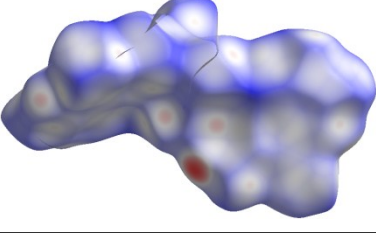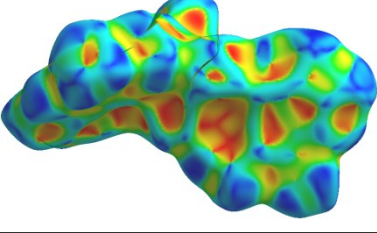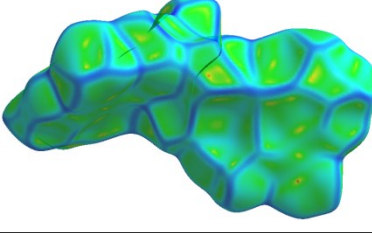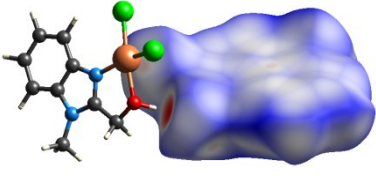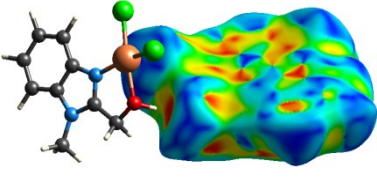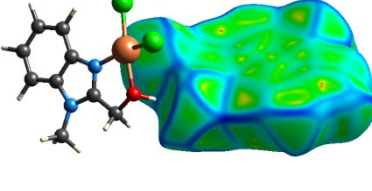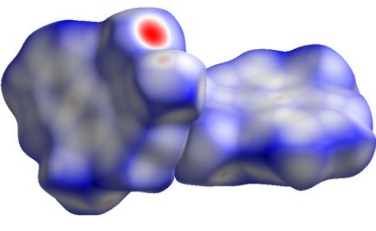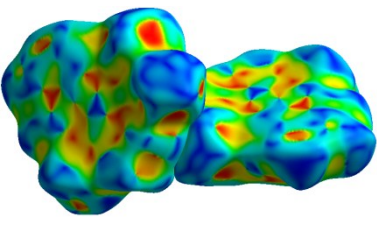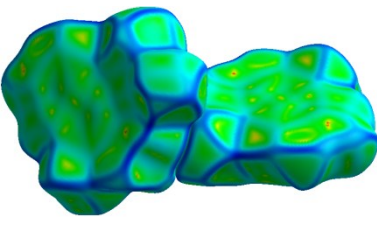
	d_{norm}	Shape Index	Curvedness
90K or 296K			
296K			

Table S9. Fingerprint plot for different interactions for **CBC** showing the percentage of contacts created to the total Hirshfeld surface area of the **CBC** molecules. d_i is the closest internal distance from a given point on the Hirshfeld surface; d_e is the closest external contact.

Inside + outside	90K	296K
All···All		
H···H 90K: 35.6% 296K: 32.4%		
Cl···H 90K: 36.6% 296K: 33.6%		
O···H 90K: 3.9% 296K: 3.5%		
N···H 90K: 2.2% 296K: 2.1%		
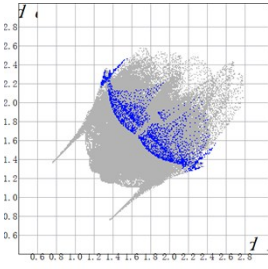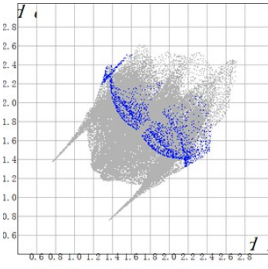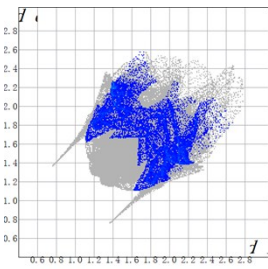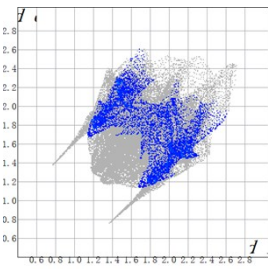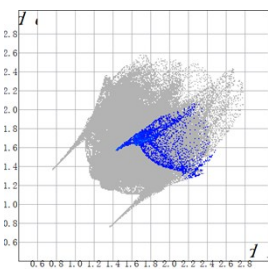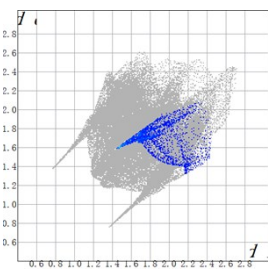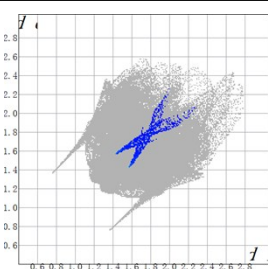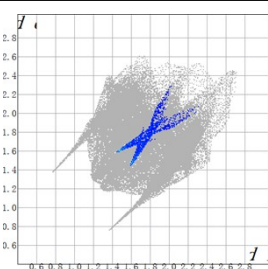
Cu···H 90K: 2.1% 296K: 2.1%		
C···H 90K: 12.1% 296K: 10.9%		
Cu···All 90K: 2.9% 296K: 2.6%		
Cu···Cl 90K: 1.6% 296K: 2.9%		

Table S10. Calculated orbitals energy for MS fragments CuL_2 (**7**), Cu_2L_2Cl (**8**), Cu_2L_3 (**9**), and $Cu_4L_4Cl_3$ (**10**).
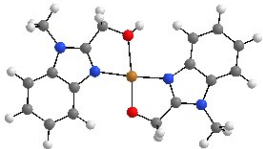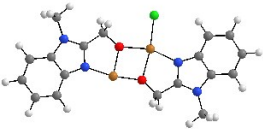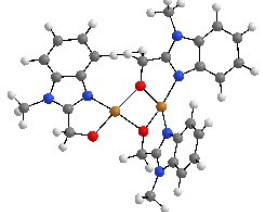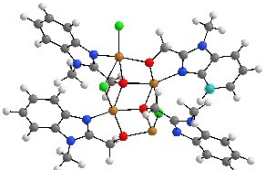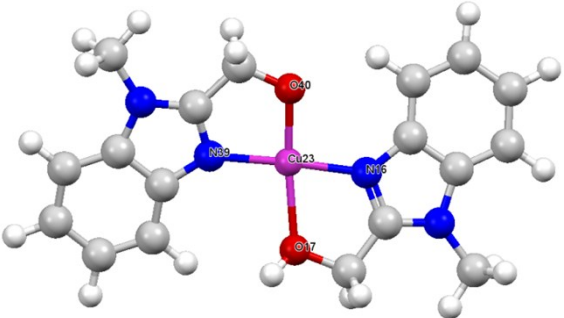
Compound	HOMO / a.u.	LUMO / a.u.	Picture	Energe / a.u.
CuL_2(**7**)	Alpha -0.34008 Beta -0.33682	Alpha -0.14479 Beta -0.21850		-1264.272529
Cu_2L_2Cl(**8**)	Alpha -0.33528 Beta -0.33462	Alpha -0.16441 Beta -0.28352		-1921.314423
Cu_2L_3(**9**)	Alpha -0.31749 Beta -0.31333	Alpha -0.13023 Beta -0.20275		-1994.343406
$Cu_4L_4Cl_3$(**10**)	Alpha -0.30822 Beta -0.30720	Alpha -0.12961 Beta -0.23439		-4303.174299

Table S11. Selected bond lengths (Å) and angles (°) for the optimized MS fragments MS fragments CuL_2 (**7**), Cu_2L_2Cl (**8**), Cu_2L_3 (**9**), and $Cu_4L_4Cl_3$ (**10**).

CuL_2 (**7**)					
Cu23-O40	1.894	Cu23-O17	2.178	Cu23-N39	1.947
Cu23-N16	1.965	O40-Cu23-N39	86.03	O40-Cu23-N16	98.91
O17-Cu23-N39	98.96	O17-Cu23-N16	77.29		

Cu₂L₂Cl (8)					
Cu22-O17	1.930	Cu22-O39	1.859	Cu22-N16	1.899
Cu44-O17	2.009	Cu44-O39	2.060	Cu44-N38	1.961
Cu44-Cl45	2.205	O17-Cu22-N16	86.00	O89-Cu22-O17	84.42
Cl45-Cu44-O17	95.43	Cl45-Cu44-N38	106.08	O17-Cu44-O89	77.45
O89-Cu44-N38	80.94				

Cu₂L₃ (9)					
Cu22-O61	1.958	Cu22-O17	1.932	Cu22-N60	1.988
Cu22-N16	1.999	Cu44-O61	2.021	Cu44-O17	1.984
Cu44-N38	1.981	Cu44-O39	1.898	N60-Cu22-N16	116.20
N60-Cu22-O61	83.04	O61-Cu22-O17	80.59	N16-Cu22-O17	83.67
O61-Cu44-O17	77.84	O61-Cu44-N38	108.23	N38-Cu44-O39	85.36
O17-Cu44-O39	93.49				

Cu₄L₄Cl₃ (10)					
Cu22-N16	1.954	Cu22-Cl91	2.380	Cu22-O17	1.987
Cu22-O39	1.899	Cu44-O84	2.465	Cu44-Cl45	2.241
Cu44-O17	1.996	Cu44-O39	2.058	Cu44-N38	2.001

Cu67-N61	1.996	Cu67-O62	1.956	Cu67-O84	1.978
Cu67-Cl91	2.391	Cu67-O17	2.587	Cu89-O62	1.988
Cu89-Cl90	2.240	Cu89-N83	1.993	Cu89-O84	2.104
Cu89-Cl45	2.882	N16-Cu22-Cl91	111.94	Cl91-Cu22-O39	102.41
N16-Cu22-O17	83.05	O17-Cu22-O39	83.53	O17-Cu44-O39	79.37
N38-Cu44-O39	79.97	O17-Cu44-Cl45	96.30	N38-Cu44-Cl45	105.06
O39-Cu44-O84	100.38	O84-Cu44-Cl45	91.49	N61-Cu67-O62	82.44
O62-Cu67-O84	82.78	N61-Cu67-Cl91	100.78	O84-Cu67-Cl91	96.64
Cl91-Cu67-O17	87.90	O17-Cu67-O62	82.62	O62-Cu89-O84	78.89
N83-Cu89-O84	80.25	O62-Cu89-Cl90	96.14	N83-Cu89-Cl90	101.32
Cl45-Cu89-Cl90	106.57	Cl45-Cu89-O84	83.61		
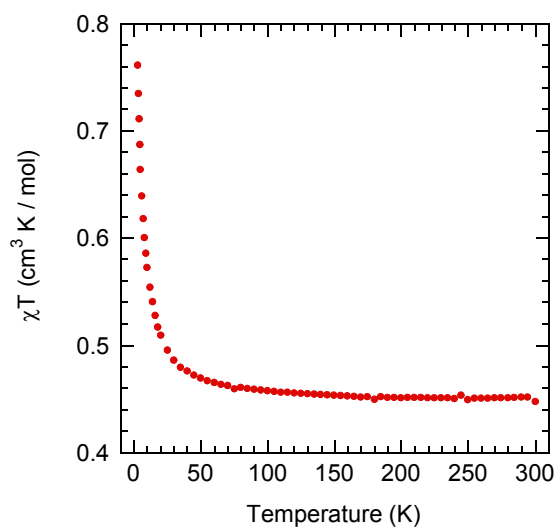
Figure S7. Temperature dependence of $\chi_m T$ for **CBC** in a static field of 1 kOe.
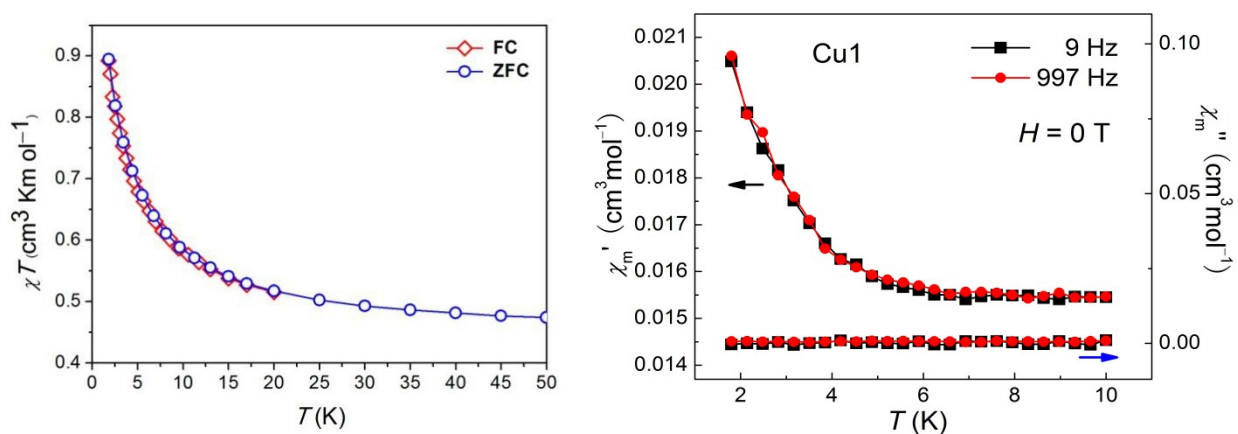
Figure S8. (Left) The FC-ZFC magnetic susceptibility of **CBC**. (Right) The temperature dependence of ac magnetic susceptibility of **CBC**.
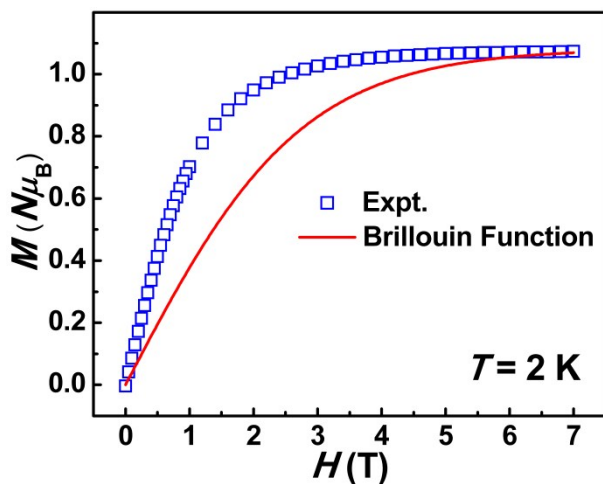
Figure S9. The isothermal magnetization of **CBC** at 2 K. The red line corresponds to the simulation employing the Brillouin function for S = 1/2 with the *g*-values from HF-EPR (g_x = 2.24, g_y = 2.16, and g_z = 2.09).
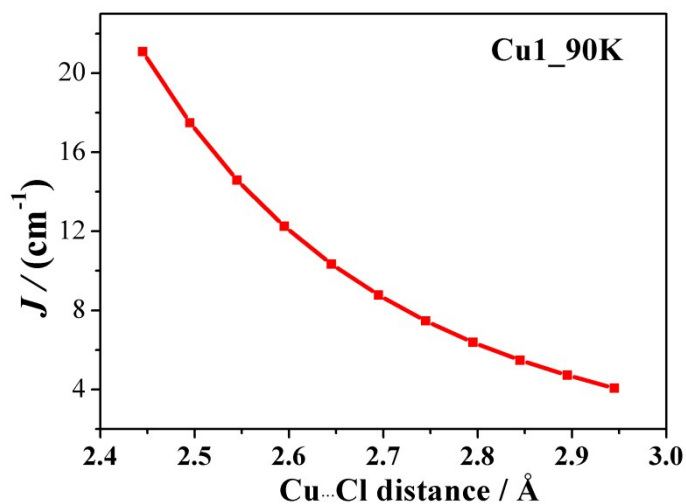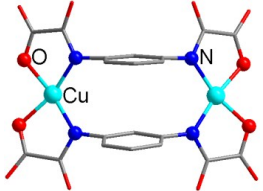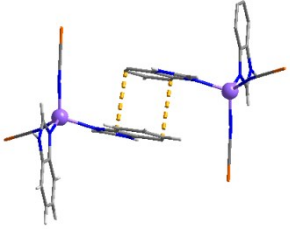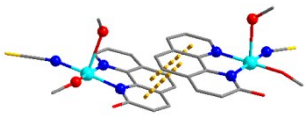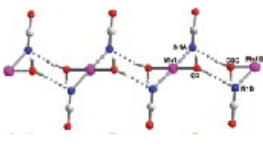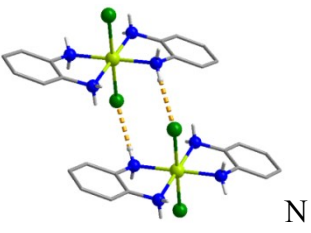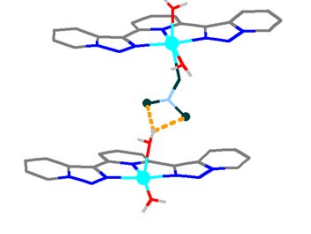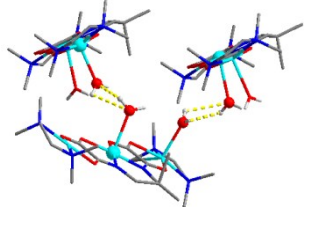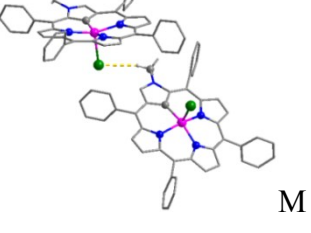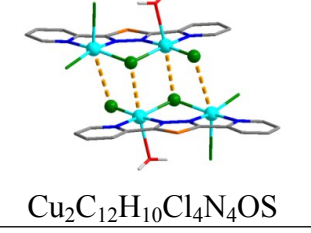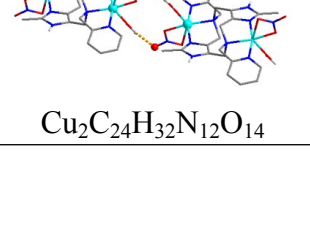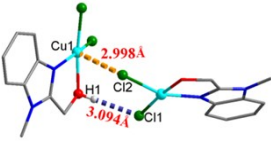

Figure S10. View of *J* value vs Cl2a···Cu1 distance. The *J* value increases with decreased Cl2a···Cu1 distance.

Table S12. Examine part of the literatures about magnetic exchange via weak interaction. (F = Ferromagnetic, AF = Antiferromagnetic, BS = broken-symmetry).

No.	Compound	M···M distance / Å	Magnetic Exchange Pathway	Magnetism	Theoretical	Reference
[1]	$Cu_2C_{20}H_{28}N_4Na_4O_{22}$	6.822(2)	Cu-N-Ph-N-Cu	F	DFT-BS	*Angew. Chem. Int. Ed.* **2001**, *40*, 3039.
[2]	$Co(bzi)_2(NSC)_2$	9.017(1)	π···π Stacking	F	DFT-BS	*Sci. Rep.* **2015**, *5*, 10761.
[3]	$Cu_2(SCN)_2(PhenOH)$ $(OCH_3)_2(HOCH_3)_2$	9.045(2)	π···π Stacking	F	DFT-BS	*Dalton Trans.* **2011**, *40*, 1453.
[4]	$MnC_{18}H_{20}N_4O_8$	4.453(3)	Hydrogen Bonding (N···H-O)	F	No	*Dalton Trans.* **2013**, *42*, 4533.
[5]	$CuF_2(H_2O)_2(pyz)$	5.331(3) 5.351(3) 6.869(1)	Hydrogen Bonding (F···H-O)	AF	DFT-BS	*Chem. Commun.* **2013**, *49*, 499.

[6]	 iC$_{12}$H$_{16}$C$_{l2}$N$_4$	5.903(2)	Hydrogen Bonding (N-H···Cl)	AF	DFT-BS	*Inorg. Chem.* **2012**, *51*, 5487.
[7]	 [Cu(TPT)(H$_2$O)$_2$(BF$_4$)]$^+$	7.441(5)	Hydrogen Bonding (F···H-O)	F	No	*CrystEng Comm* **2013**, *15*, 1836.
[8]	 Cu$_3$C$_{21}$H$_{48}$F$_{12}$N$_6$O$_9$P$_2$	6.202(1)	Hydrogen Bonding (O···H-O)	F	DFT-BS	*Inorg. Chem.* **2002**, *41*, 5373.
[9]	 nC$_{45}$H$_{30}$N$_4$Br	9.558(2)	Hydrogen Bonding (C-H···Br)	F	No	*Inorg. Chem.* **2008**, *47*, 7202.
[10]	 Cu$_2$C$_{12}$H$_{10}$Cl$_4$N$_4$OS	4.283(5)	Chloride Neighbor Cu-Cl···Cu	AF	DFT-BS	*Inorg. Chem.* **2004**, *43*, 1865.
[11]	 Cu$_2$C$_{24}$H$_{32}$N$_{12}$O$_{14}$	6.255(2)	Hydrogen Bonding	AF	DFT-BS	*Inorg. Chem.* **2011**, *50*, 5696.

[12]	Cu(C$_9$H$_{10}$N$_2$O)Cl$_2$	4.581(9)	Cu-Cl···Cu Cu-O-H···Cl-Cu	F	DFT-BS	**This work**